JOURNAL OF GEOPHYSICAL RESEARCH, VOL. 96, SUPPLEMENT, PAGES 3425–3436, FEBRUARY 28, 1991

On the Two-Phase Thermodynamics of the Coupled Cloud-Ocean Mixed Layer

P. C. CHU AND R. W. GARWOOD, JR.

Department of Oceanography, Naval Postgraduate School, Monterey, California

The rudiments of a self-consistent two-phase thermodynamical theory of intraseasonal and interannual variability for the tropical cloud-ocean mixed layer system are presented. In this paper we study some basic properties of low-frequency phenomena in the tropical coupled cloud-ocean mixed layer system under low mean wind speed conditions and attempt to seek a unified thermodynamical framework in which the thermodynamical oscillation can be studied and understood. In order to do so, all waves in the atmosphere and in the ocean are initially filtered out, and the coupled system is purely thermodynamic. An air-ocean coupled model designed especially for the low wind speed condition is employed to test the basic thermodynamic feedback mechanism between clouds and the ocean mixed layer. The model has four parts: (1) a shallow-water system for the large-scale atmosphere motion; (2) a cloud model, (3) a marine atmospheric boundary layer, in which the physical processes are parameterized into the bulk formulae through a geostrophic drag coefficient and corresponding heat and moisture exchange coefficients; and (4) an oceanic mixed layer model. The coupled model is solved analytically as an eigenvalue problem. Three nondimensional model parameters are found to be very important in separating growing or decaying, oscillatory or nonoscillatory modes: (1) the ocean surface stability index, ε; (2) the surface water budget index, γ; and (3) the mean diapycnal gradient of the spiciness (χ) in the entrainment zone, δ. The sign of ε divides the ocean mixed layer into shallowing ($\varepsilon > 0$) and entrainment ($\varepsilon < 0$) regimes. The value of γ indicates the strength of the water budget versus the heat budget at the ocean surface. The net freshwater influx (e.g., precipitation exceeding evaporation) destabilizes the coupled cloud and ocean mixed layer. In the entrainment regime, however, the parameter δ becomes important. The unstable oscillation only appears when the entrainment zone is salinity dominated. When δ exceeds a criterion that depends upon ε and γ, the oscillatorily growing modes will be generated. The model results show that the criteria are: $\delta > 20\varepsilon + 11$ for $\gamma = -0.1$, $\delta > 20\varepsilon + 11.8$ for $\gamma = -0.2$, and $\delta > 20\varepsilon + 14.6$ for $\gamma = -0.5$. The model results also demonstrate that the exchanges of heat and water across the sea surface lead to both growing and decaying modes of oscillation on two different time scales, owing to the stability of the atmosphere. For an unstable atmosphere the time scale is about 20–30 days. However, the time scale is approximately 1–3 years for a stable atmosphere. This work introduces the new concept of two-phase thermodynamics for the coupled air-ocean system. Both atmosphere and ocean have two important thermodynamical variables: temperature and moisture (or fractional cloudiness) for the atmosphere, and temperature and salinity for the ocean. If salinity is neglected in the ocean model, no positive feedback mechanism will be possible in the coupled air-ocean system.

1. INTRODUCTION

The ocean mixed layer and clouds are coupled by the fluxes of heat and water mass at the interface. The importance of the fluxes of momentum and heat is well recognized by both meteorologists and oceanographers. However, the water mass flux has been given considerable attention only in atmospheric models, since the latent heat release is an important source of energy for the atmospheric general circulation. The water mass flux has been given less attention in ocean models, although it is realized that evaporation and precipitation contribute to the surface buoyancy flux that influences the depth of mixing and the thermohaline circulation.

In a series of papers, *Chu and Garwood* [1989, 1990] and *Chu et al.* [1990] presented positive and negative feedback mechanisms between clouds and the ocean mixed layer. First, clouds reduce the incoming solar radiation at the ocean surface by scattering and absorption, which cools (relatively) the ocean surface layer by increasing mixed layer entrainment. The cooling of the ocean mixed layer lowers the evaporation rate, which will diminish the clouds. This is a negative feedback mechanism. Second, precipitation dilutes the surface salinity, stabilizing the upper ocean and reducing mixed layer deepening. The mixed layer may be caused to shallow if the downward surface buoyancy flux is sufficiently enhanced by the precipitation. The reduction in mixed layer depth will increase the sea surface temperature (SST) by concentrating the net radiation plus heat fluxed downward across the sea surface into a thinner layer. The increase of SST augments the surface evaporation, which in turn produces more clouds. This is a positive feedback mechanism. Figure 1 illustrates the feedback pathways between the clouds and the ocean mixed layer. The feedback mechanism between clouds and the ocean mixed layer depends largely on the thermodynamics of the ocean mixed layer. *Chu and Garwood* [1990] and *Chu et al.* [1990] predict the excitation of oscillatorily and exponentially growing modes under the strong surface wind (~ 10 m s^{-1}) condition with two different time scales: (20–30 days, 1–3 years), that largely depend on the static stability of the marine atmospheric boundary layer (MABL). For the unstable MABL, the time scale is 20–30 days, and for the stable MABL, the time scale is 1–3 years.

In the near-equatorial region northeast of New Guinea, the long-term monthly mean wind speeds are of order 1 m s^{-1} [*Sadler et al.*, 1978]. The magnitude of the annual average

This paper is not subject to U.S. copyright. Published in 1991 by the American Geophysical Union.

Paper number 90JC01862.

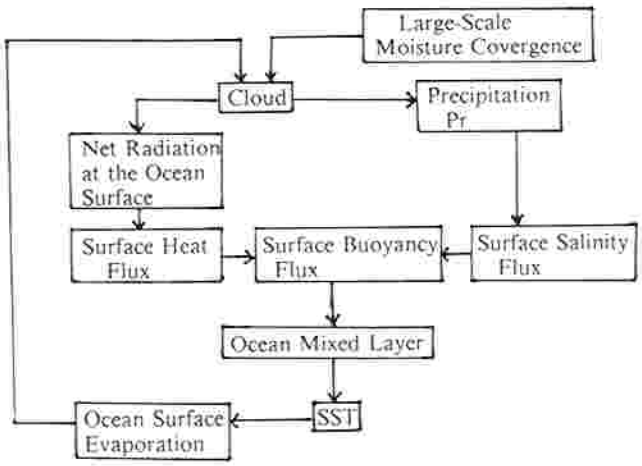

Fig. 1. Feedback paths between OPBL and clouds.

vector wind stress for the region 4°N–4°S, 140°–160°E is given by *Wyrtki and Meyers* [1976] as 2.5×10^{-3} N m^{-2}, roughly equivalent to a mean wind speed of 1.2 m s^{-1}. It remains to be determined whether the feedback mechanism between clouds and the ocean mixed layer of *Chu and Garwood* [1990] is still important under such weak wind forcing. In such a case, the ocean surface buoyancy flux becomes a dominating factor for either generating or dampening of the turbulent kinetic energy in the upper ocean, depending upon the sign of the buoyancy flux. Upward buoyancy flux causes the water column to be statically unstable, which generates turbulence. On the other hand, downward buoyancy flux makes the water column statically stable, damping the turbulence. In the case of upward buoyancy flux, the mixed layer entrains water from below, increasing the potential energy. In the case of a strong downward buoyancy flux and weak winds, the turbulence kinetic energy budget is dominated by buoyant damping, and there is insufficient shear production to provide energy for entrainment. Hence the mixed layer is assumed to remain at or to be close to a steady state, with negligible entrainment fluxes (relative to the surface fluxes of heat and water). It is expected that the effect of clouds on the ocean mixed layer is different for the stable and unstable regimes.

Although our coupled model is a one-dimensional box model, we are aware of the importance of horizontal advection and the limitations of one-dimensional models. However, the intent of this work is to develop a formalism to examine thermodynamic feedback between the two fluids. Because we wish to concentrate on the thermodynamic interaction, horizontal advection is either prescribed or ignored initially.

2. ATMOSPHERIC MODEL

The atmospheric model is a combination of three parts: (1) a shallow-water system for the large-scale atmospheric motion, (2) a cloud model, and (3) a marine atmospheric boundary layer, in which the physical processes are parameterized into the bulk formulae through a geostrophic drag coefficient and corresponding heat and moisture exchange coefficients. A shallow-water system for the atmosphere is given by [cf. *Gill*, 1980; *Davey*, 1985; *Lau and Shen*, 1988]:

$$\frac{\partial u_a'}{\partial t_0} - \bar{\beta} y v_a' = \frac{g H_a}{\bar{\theta}_a} \frac{\partial \theta_a}{\partial x} - D_m u_a' \tag{1a}$$

$$\frac{\partial v_a'}{\partial t_0} + \bar{\beta} y u_a' = \frac{g H_a}{\bar{\theta}_a} \frac{\partial \theta_a'}{\partial y} - D_m v_a' \tag{1b}$$

$$\frac{g H_a}{\bar{\theta}_a} \frac{\partial \theta_a'}{\partial t_0} - N^2 H_a^2 \left(\frac{\partial u_a'}{\partial x} + \frac{\partial v_a'}{\partial y} \right) = Q_a' - \frac{D_T g H_a}{\bar{\theta}_a} \theta_a' \tag{1c}$$

$$\left[\Lambda_a h_c \frac{\partial n'}{\partial t_0} + (1 - \Lambda_a) \frac{\partial q'}{\partial t_0} \right] + [\Lambda_a q_s + (1 - \Lambda_a) q_0] \cdot \left(\frac{\partial u_a'}{\partial x} + \frac{\partial v_a'}{\partial y} \right) = E' - P_r' \tag{1d}$$

$$\frac{\partial}{\partial t_0} = \frac{\partial}{\partial t} + \bar{U}_a \frac{\partial}{\partial x} + \bar{V}_a \frac{\partial}{\partial y} \tag{1e}$$

where $\bar{U}_a$ and $\bar{V}_a$ are the mean zonal and meridional velocity of the lower atmosphere, respectively; u_a' and v_a' are the zonal and meridional perturbation velocity of the lower atmosphere, respectively; θ_a' is the perturbation tropospheric temperature; n' is the perturbation fractional cloudiness; q' is the perturbation moisture content, which is expressed as depth of liquid water per unit area and related to background moisture q_0; q_s is the saturated moisture content; H_a and $\bar{\theta}_a$ represent the mean depth of the lower layer and the mean potential temperature, respectively; N_a and Q_a' represent the buoyancy frequency and the perturbation heating; E' is the ocean surface evaporation rate; P_r' is the precipitation rate; h_c is the total amount of water vapor needed to create a cloud over a unit area; and $\bar{\beta}(= df/dy)$ is the latitudinal gradient of the Coriolis parameter. From the mean distributions of temperature and moisture content in the environmental air outside the cloud and inside a deep cumulus cloud [*Kuo*, 1965], we estimate that $h_c \sim 5$ cm.

The perturbation moisture content q' and the perturbation cloud cover n' are computed for two regimes: convective and nonconvective. For the convective regime ($\Lambda_a = 1$), (1*d*) becomes the prognostic equation for the fractional cloudiness:

$$h_c \frac{\partial n'}{\partial t_0} + q_s \left(\frac{\partial u_a'}{\partial x} + \frac{\partial v_a'}{\partial y} \right) = E' - P_r' \tag{2a}$$

where n' is treated as the perturbation in fraction of clouds over certain subgrid areas in the large-scale atmospheric system. In order to incorporate the satellite data into the model, the subgrid areas are chosen to be 1.5° × 1.5° (168 km × 168 km) boxes. The time rate of change of fractional cloudiness is proportional to the moisture supply in each box, divided by the amount of water vapor necessary to produce clouds in the box. The main processes causing the cloud dissolution are precipitation and mixing with the environmental air. The cloud evaporation due to mixing with ambient air is a complicated problem and is neglected here for the sake of simplicity. For the nonconvective regime ($\Lambda_a = 0$), (1*d*) becomes the moisture transport equation:

$$\frac{\partial q'}{\partial t_0} + q_0\left(\frac{\partial u_a'}{\partial x} + \frac{\partial v_a'}{\partial y}\right) = E' - P_r' \tag{2b}$$

Following *Lau and Shen* [1988], the heating rate Q_a' in the convective regime is related to the precipitation rate by

$$Q_a' = \Lambda_a \eta N H_a P_r' \tag{3}$$

where

$$\eta \equiv \frac{g\rho_w L_v}{\bar{\theta}_a \rho_a c_{pa} N H_a}$$

which is treated as a constant in this research.

By linear regression of hourly rain amount and satellite IR brightness data obtained during phases I, II, and III of the Global Atlantic Tropical Experiment (GATE), *Albright et al.* [1985] suggested a linear relationship between precipitation rate averaged in the boxes and fractional cloudiness n of the boxes by clouds with tops colder than −36°C:

$$P_r\ (\mathrm{m\ s^{-1}}) = (0.472 + 8.333n) \times 10^{-7} \tag{4a}$$

This result verified *Arkin*'s [1979] earlier analysis for the GATE B-scale array. From (4*a*) we obtain a linear relationship between perturbation precipitation P_r' and perturbation fractional cloudiness n':

$$P_r' = \Lambda_a \xi n' \qquad \xi \equiv \frac{\partial \bar{P}_r}{\partial n} = 8.333 \times 10^{-7}\ \mathrm{m\ s^{-1}} \tag{4b}$$

In order to filter out all atmospheric waves, we assume

$$\frac{\partial}{\partial t_0}(u_a', v_a', \theta_a', n') = 0 \tag{5}$$

and, after using (3) and (4*b*), (1*a*)–(1*d*) become

$$-\bar{\beta} y v_a' = \frac{gH_a}{\bar{\theta}_a}\frac{\partial \theta_a'}{\partial x} - D_m u_a' \tag{6a}$$

$$\bar{\beta} y u_a' = \frac{gH_a}{\bar{\theta}_a}\frac{\partial \theta_a'}{\partial y} - D_m v_a' \tag{6b}$$

$$-N^2 H_a^2\left(\frac{\partial u_a'}{\partial x} + \frac{\partial v_a'}{\partial y}\right) = \Lambda_a N H_a \eta \xi n' - \frac{D_T g H_a}{\bar{\theta}_a}\theta_a' \tag{6c}$$

$$[\Lambda_a q_s + (1 - \Lambda_a) q_0]\left(\frac{\partial u_a'}{\partial x} + \frac{\partial v_a'}{\partial y}\right) = E' - \Lambda_a \xi n' \tag{6d}$$

which are basic equations for the four unknowns u_a', v_a', θ_a', and n'. After solving (6*a*) and (6*b*) as algebraic equations for u_a' and v_a', we compute the divergence of the perturbation wind field

$$\frac{\partial u_a'}{\partial x} + \frac{\partial v_a'}{\partial y} = \frac{D_m}{D_m^2 + \beta^2 y^2}\nabla^2\theta_a' - \frac{\bar{\beta}}{D_m^2 + \beta^2 y^2}\frac{\partial \theta_a'}{\partial x} - \frac{2\bar{\beta}^2 y}{(D_m^2 + \bar{\beta}^2 y^2)^2}\left(D_m \frac{\partial \theta_a'}{\partial y} - \bar{\beta} y \frac{\partial \theta_a'}{\partial x}\right) \tag{7a}$$

If our model is applied to the equatorial region, we may assume $y \sim 0$ in (7*a*), which leads to

$$\frac{\partial u_a'}{\partial x} + \frac{\partial v_a'}{\partial y} = \frac{1}{D_m}\left(\nabla^2 - \frac{\bar{\beta}}{D_m}\frac{\partial}{\partial x}\right)\theta_a' \tag{7b}$$

Equations (6*c*), (6*d*), and (7*b*) are the basic equations for three variables: n', θ_a', and $\partial u_a'/\partial x + \partial v_a'/\partial y$. Eliminating the last two variables from (6*c*), (6*d*), and (7*b*), we obtain a diagnostic equation for the perturbation fractional cloudiness in the subgrid boxes:

$$\mathcal{R}\left\{\Lambda_a \xi\left[\eta - \frac{1}{\Lambda_a q_s + (1 - \Lambda_a) q_0}\right] n' + \frac{E'}{\Lambda_a q_s + (1 - \Lambda_a) q_0}\right\} + \frac{\Lambda_a D_T D_m \eta \xi}{N^2 H_a^2} n' = 0 \tag{8}$$

where $\mathcal{R}$ is a second-order differential operator defined by

$$\mathcal{R} \equiv \nabla^2 - \frac{\bar{\beta}}{D_m}\frac{\partial}{\partial x} - \frac{D_T D_m}{N^2 H_a^2}$$

For slow damping in the atmosphere (i.e., small D_T, D_m), the fractional cloudiness equation (8) is simplified as

$$\Lambda_a \xi\left[\eta - \frac{1}{\Lambda_a q_s + (1 - \Lambda_a) q_0}\right] n' - \frac{E'}{\Lambda_a q_s + (1 - \Lambda_a) q_0} = 0 \tag{9}$$

In the convective regime ($\Lambda_a = 1$), the fractional cloudiness equation becomes

$$n' = \frac{E'}{\xi[1 - \hat{e}(\bar{T}_s)]} = \frac{\partial \bar{E}/\partial T_s}{\xi[1 - \hat{e}(\bar{T}_s)]} T_s' \tag{10}$$

where

$$\hat{e}(\bar{T}_s) \equiv \eta q_s(\bar{T}_s)$$

and $\bar{T}_s$ is the mean SST. *Lau and Shen* [1988] define $e(T_s)$ as the SST-dependent moisture factor, with values from 0 to 1. In the convective regime, $P_r' = \xi n'$, (10) becomes

$$-\xi \hat{e}(\bar{T}_s) n' = E' - P_r'$$

With a long-time average, the perturbation model variables, including fractional cloudiness (n') and ocean mixed layer temperature (T_s'), should be zero, which means

$$\int_{\Delta t} (E' - P_r')\, dt = 0$$

with a reasonable value of Δt.

3. EFFECTS OF CLOUDS ON OCEAN SURFACE BUOYANCY FLUX

For the case of an ocean surface without ice (low and middle latitudes) the downward ocean surface buoyancy flux (B) has two components:

$$B = -\frac{\alpha g F}{\rho_{w0} c_{pw}} + \beta g (P_r - E) S \tag{11}$$

Here α is the seawater thermal expansion coefficient, β is the salinity contraction coefficient, ρ_{w0} is the characteristic seawater density, c_{pw} is the seawater specific heat under

constant pressure, and F is the upward heat flux plus net radiation across the air-ocean interface. The expressions that follow are for the net upward heat flux at the ocean surface,

$$F = R_b - R_s + L_v \rho_w E + H_s \tag{12a}$$

for the surface evaporation,

$$E = \rho_a U_g C_E [q_s(T_s) - q]/\rho_w \tag{12b}$$

and for the sensible heat flux from the ocean surface,

$$H_s = \rho_a c_{pa} U_g C_H (T_s - \theta_a) \tag{12c}$$

where U_g is the geostrophic wind. C_g and C_H are the geostrophic drag coefficient and heat exchange coefficient, defined by *Yamada* [1976],

$$C_g = \frac{u_{\bar{a}*}}{U_g} = \kappa \left\{ \left[\ln\left(\frac{h_a}{z_0}\right) - \bar{a} \right]^2 + \bar{b}^2 \right\}^{-1/2} \tag{13a}$$

$$C_H = = \frac{\kappa C_g}{Pr_0} \left[\ln\left(\frac{h_a}{z_0}\right) - \bar{c} \right]^{-1} \tag{13b}$$

where the von Karman constant is $\kappa = 0.4$. The roughness parameter (z_0) is approximately 1.5×10^{-4} m. The ratio h_a/z_0 is 0.6×10^7 for an MABL height, $h_a = 1$ km. Pr_0 is the turbulent Prandtl number for neutral stability, having a value of 0.74 according to *Businger et al.* [1971]. The parameters $\bar{a}$, $\bar{b}$, and $\bar{c}$ are experimentally determined similarity functions. On the basis of the Wangara data, *Yamada* [1976] found the analytical forms of $\bar{a}$, $\bar{b}$, and $\bar{c}$ as functions of the instability parameter h_a/L_a, where L_a is the atmospheric Obukhov length scale. It is noteworthy that the definition of the geostrophic drag here is different from the quadratic law ($u_{\bar{a}*}^2 = C_g U_g^2$), and that the determination of the analytical forms of $\bar{a}$, $\bar{b}$, and $\bar{c}$ were obtained from the Wangara atmospheric boundary layer over land, rather than over oceans. There have been no comparable observations in the MABL as yet. Nevertheless, we assume that these similarity functions are valid for the MABL. Furthermore, since the computation method for the moisture transfer coefficient is not well established, in this study we assume that $C_E = C_H$. Substitution of $\bar{a}$, $\bar{b}$, and $\bar{c}$ into (14*a*) and (14*b*) leads to apparently strong dependence of C_g, C_H, C_E on the atmospheric stability parameter h_a/L_a, as shown in Figure 2. These parameters have much larger values for the unstable atmosphere than for the stable atmosphere, i.e.,

$$C_g \sim 3.16 \times 10^{-2}, \quad C_H, C_E \sim 2 \times 10^{-3} \quad h_a/L_a < 0$$

$$C_g \sim 3 \times 10^{-3}, \quad C_H, C_E \sim 1.24 \times 10^{-5} \quad h_a/L_a > 0$$

The perturbation surface heat flux F' is computed by

$$F' = \frac{\partial \bar{F}}{\partial n} n' + \frac{\partial \bar{F}}{\partial T_s} T_s' + \frac{\partial \bar{F}}{\partial q} q' + \frac{\partial \bar{F}}{\partial \theta_a} \theta_a'$$

The four terms in the right-hand side of this equation indicate cloud-radiation feedback, SST-evaporation feedback, moisture-evaporation feedback, and air temperature–heat flux feedback, respectively. Among them, the first two feedback mechanisms directly affect the coupled cloud-ocean mixed layer system. In order to simplify the system, we consider

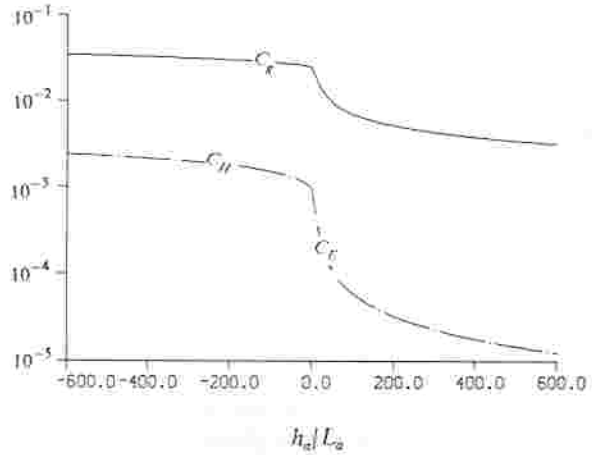

Fig. 2. Dependence of C_D, C_E, C_H on the atmospheric stability parameter (h_a/L_a).

only the cloud-radiation and SST-evaporation feedback in this paper. Therefore

$$F' = \frac{\partial \bar{F}}{\partial n} n' + \frac{\partial \bar{F}}{\partial T_s} T_s' \tag{14}$$

The effect of clouds on the buoyancy flux at the ocean surface is twofold: (1) decreasing B through the increase in the net heat loss at the ocean surface (F) by reducing the net radiation at ocean surface (cloud-radiation feedback), and (2) increasing B due to precipitation. The variation of fractional cloudiness generally changes each term in the right-hand side of (12*a*), i.e., longwave back radiation, (R_b), solar radiation (R_s), evaporation (E), and sensible heat flux (H_s). Among them, only the radiation budget is directly affected by cloudiness; the latent and sensible heat fluxes are indirectly influenced by cloudiness through the change in SST. Cloud-radiation feedback contains albedo (reduction of solar radiation) and greenhouse (emission of downward longwave radiation) effects. Averaging the total cloud-radiative forcing predicted by several general circulation models [*Stephens*, 1989, Table 2], we obtain

$$\frac{\partial \bar{F}}{\partial n} = \frac{\partial}{\partial n} (R_b - R_s) \sim 17 \text{ W m}^{-2} \tag{15}$$

which means the domination of albedo effect over greenhouse effect.

The variation in SST will mainly change the longwave back radiation and the sensible and latent heat fluxes; therefore from (12*a*), (12*b*), and (12*c*), we can expect

$$\frac{\partial \bar{F}}{\partial T_s} = \rho_a c_{pa} U_g \left(1 + \frac{L_v^2 q_s}{c_{pa} R_v \bar{T}_s^2} \frac{C_E}{C_H} + \frac{4\sigma_{SB} \bar{T}_s^3}{\rho_a c_{pa} U_g C_H} \right) C_H \tag{16}$$

where the Stefan-Boltzmann constant is $\sigma_{SB} = 5.67 \times 10^{-8}$ W m^{-2} K^{-4}

4. Ocean Mixed Layer Model

Most models that include thermodynamic effects regard the upper layer as a well-mixed turbulent boundary layer which exchanges heat and moisture with the atmosphere and

entrains water from below. The heat and salinity equations take the forms

$$h_w \frac{\partial T_s}{\partial t} = -w_e(T_s - T_{-h}) - \frac{F}{\rho_{w0} c_{pw}} + A_T \qquad (17a)$$

$$h_w \frac{\partial S}{\partial t} = -w_e(S - S_{-h}) + (E - P_r)S + A_S \qquad (17b)$$

where h_w is the mixed layer depth; T_{-h} and S_{-h} are temperature and salinity at the base of the mixed layer, respectively; and A_T and A_S are the horizontal advection for temperature and salinity, respectively. The entrainment velocity is w_e and is parameterized by *Chu and Garwood* [1988] as

$$w_e = \Lambda_w \frac{(C_1 u_{w*}^3 - C_2 Bh)}{gh[\alpha(T_s - T_{-h}) - \beta(S - S_{-h})]} \qquad (18)$$

where C_1 and C_2 are tuning coefficients, and u_{w*} is the water surface friction velocity, which is computed by

$$u_{w*} = \left(\frac{\rho_a}{\rho_{w0}}\right)^{1/2} u_{a*} \qquad (19)$$

Considering the low-wind case only, we set $u_{a*} \sim 3$ cm s^{-1}, $u_{w*} \sim 0.1$ cm s^{-1}. The symbol Λ_w is a Heaviside function of $(C_1 u_{w*}^3 - C_2 Bh)$. When $(C_1 u_{w*}^3 - C_2 Bh) > 0$, there is sufficient turbulent kinetic energy to entrain and mix water from below and $\Lambda_w = 1$, which represents the entrainment regime. The entrainment rate is determined by (18) and is substituted into (20) to prognosticate the mixed layer depth h_w:

$$\frac{\partial h_w}{\partial t} = w_e - w_{-h} \qquad (20)$$

Here w_{-h} is the mean vertical velocity at the mixed layer base.

When $(C_1 u_*^3 - C_2 Bh) < 0$, there is insufficient turbulent kinetic energy to entrain water from below, and w_e is set to be zero, i.e., $\Lambda_w = 0$. This is called the surface damping regime. The mixed layer depth is calculated diagnostically from a balance of the remaining terms in (18), and it equals the oceanic Obukhov length scale, L_w:

$$h_w = L_w = \frac{C_1 u_{w*}^3}{C_2 B} \qquad (21a)$$

The surface damping regime occurs when the buoyancy gain due to excess precipitation prevails over the buoyancy lost by ocean surface cooling. The mean mixed depth in the surface damping regime is computed by

$$\bar{h}_w = \frac{C_1 \bar{u}_{w*}^3}{C_2 \bar{B}} \qquad (21b)$$

The temperature and salinity equations (17*a*) and (17*b*) prescribe the balance of storage, entrainment, and heat/water mass flux.

If we use two orthogonal variables (ρ_w, χ) in the TS diagram instead of (T_s, S),

$$\rho_w = \rho_{w0}(\beta S - \alpha T) \qquad \chi = \rho_{w0}(\beta S + \alpha T) \qquad (22)$$

The entrainment velocity equation (18) can be simplified by

$$w_e = -\Lambda_w \rho_{w0} \frac{(C_1 u_{w*}^3 - C_2 Bh)}{gh(\rho_w - \rho_{-h})} \qquad (18')$$

where χ is "spiciness" [*Munk*, 1981]. From (17*a*), (17*b*), and (18′), we obtain two prognostic equations for density and spiciness:

$$h_w \frac{\partial \rho_w}{\partial t} = \rho_{w0}\Lambda_w \frac{(C_1 u_{w*}^3 - C_2 Bh_w)}{gh_w} - \frac{\rho_{w0} B}{g} + \rho_{w0}(\beta A_s - \alpha A_T) \qquad (23a)$$

$$h_w \frac{\partial \chi}{\partial t} = \rho_{w0}\Lambda_w \frac{(C_1 u_{w*}^3 - C_2 Bh_w)}{gh_w} \frac{\chi - \chi_{-h}}{\rho_w - \rho_{-h}} + \frac{\rho_{w0} D}{g} + \rho_{w0}(\beta A_s + \alpha A_T) \qquad (23b)$$

where

$$D = -\frac{\alpha g F}{\rho_{w0} c_{pw}} + \beta g(E - P_r)S \qquad (24)$$

is the spiciness flux at the ocean surface, which is orthogonal to the buoyancy flux (11). The ratio

$$\delta \equiv \frac{\bar{\chi} - \chi_{-h}}{\bar{\rho}_w - \rho_{-h}} = \frac{\beta(\bar{S} - S_{-h}) + \alpha(\bar{T}_s - T_{-h})}{\beta(\bar{S} - S_{-h}) - \alpha(\bar{T}_s - T_{-h})} \qquad (25)$$

is the mean diapycnal gradient of the spiciness [*Veronis*, 1972], and is taken as a model parameter in this study. It categorizes the entrainment zone: (1) $\delta = 0$, equal importance for temperature and salinity stratification; (2) $\delta > 0$, salinity stratification dominates; (3) $\delta < 0$, temperature stratification dominates.

5. PERTURBATION EQUATIONS

The mean state of the coupled cloud-OPBL (oceanic planetary boundary layer) system is evaluated from the steady state solutions for the equations (23*a*), (23*b*), (18), (20), and (21*b*).

When the coupled system is perturbed from its equilibrium state, the thermodynamic feedback mechanism between the cumulus clouds and the oceanic mixed layer either causes the perturbation to grow (positive feedback) or to dampen (negative feedback). The principal purpose here is to study possible one-dimensional thermodynamic feedback mechanisms between clouds and the oceanic mixed layer, within the limitations of the simplifying assumptions. Hence the energy exchange at the air-ocean interface is a primary focal point. Therefore we shall neglect initially the perturbations of those variables not directly related to the exchange at the air-ocean interface, such as the perturbations of the horizontal advection A_T' and A_S', the perturbations of the atmospheric variables at the top of the MABL, q' and θ_a', and the perturbations of the oceanic variables at the base of the OPBL, w'_{-h}, T'_{-h}, and S'_{-h}. From the basic equations of the coupled system (23*a*), (23*b*), (18′), and (20) or (21*a*), the equations for ρ_w', χ' are

$$\frac{\partial \rho_w'}{\partial t} = \frac{\rho_{w0}(1 + C_2\Lambda_w)}{g\bar{h}_w}\left[-B' + \frac{\bar{B}}{\bar{h}_w} h_w'\right] \qquad (26a)$$

$$\frac{\partial \chi'}{\partial t} = \frac{C_2 \Lambda_w \rho_{w0} \delta}{g \bar{h}_w} B' + \frac{\rho_{w0}}{g \bar{h}_w} D' + \frac{\rho_{w0} \bar{B}}{g \bar{h}_w} \left[C_2 \Lambda_w \delta - \frac{\bar{D}}{\bar{B}} \right] \frac{h'_w}{\bar{h}_w} \tag{26b}$$

$$\Lambda_w \frac{\partial h'_w}{\partial t} = \frac{C_2 \rho_{w0} \bar{B}}{g \Delta \rho_w} \frac{h'_w}{\bar{h}_w} + \frac{C_2 \rho_{w0}}{g \Delta \rho_w} B' - \Lambda_w \frac{\bar{w}_{-h}}{\Delta \rho_w} \rho'_w \tag{26c}$$

where

$$\Delta \rho_w = \bar{\rho}_w - \rho_{-h}$$

is the mean density jump at the base of the mixed layer, and B' and D' are perturbations of surface buoyancy and spiciness fluxes, which are computed by

$$B' = \left(\overline{\frac{\partial B}{\partial n}} \right) n' + \left(\overline{\frac{\partial B}{\partial T_s}} \right) T'_s + \beta g (\bar{P}_r - E) S' \tag{27a}$$

$$D' = \left(\overline{\frac{\partial D}{\partial n}} \right) n' + \left(\overline{\frac{\partial D}{\partial T_s}} \right) T'_s - \beta g (\bar{P}_r - \bar{E}) S' \tag{27b}$$

If the low surface wind condition is considered (especially for the western Pacific warm pool region), it is reasonable to assume that the upwelling velocity (w_{-h}) is also a negligible quantity. We may drop the last term on the right-hand side of (26c) for the first approximation.

The definitions of surface buoyancy and spiciness fluxes (11) and (24) lead to

$$\left(\overline{\frac{\partial B}{\partial n}} \right) = -\frac{\alpha g}{\rho_{w0} c_{pw}} \frac{\partial \bar{F}}{\partial n} + \beta g \bar{S} \frac{\partial \bar{P}_r}{\partial n} = -\frac{\alpha g}{\rho_{w0} c_{pw}} \frac{\partial \bar{F}}{\partial n} (1 - A) \tag{28a}$$

$$\left(\overline{\frac{\partial D}{\partial n}} \right) = -\frac{\alpha g}{\rho_{w0} c_{pw}} \frac{\partial \bar{F}}{\partial n} - \beta g \bar{S} \frac{\partial \bar{P}_r}{\partial n} = -\frac{\alpha g}{\rho_{w0} c_{pw}} \frac{\partial \bar{F}}{\partial n} (1 + A) \tag{28b}$$

$$\frac{\partial \bar{B}}{\partial T_s} = -\frac{\alpha g}{\rho_{w0} c_{pw}} \frac{\partial \bar{F}}{\partial T_s} - \beta g \bar{S} \frac{\partial \bar{E}}{\partial T_s} \tag{28c}$$

$$\frac{\partial \bar{D}}{\partial T_s} = -\frac{\alpha g}{\rho_{w0} c_{pw}} \frac{\partial \bar{F}}{\partial T_s} + \beta g \bar{S} \frac{\partial \bar{E}}{\partial T_s} \tag{28d}$$

where

$$A \equiv \frac{\rho_{w0} c_{pw} \beta \xi \bar{S}}{\alpha \partial \bar{F} / \partial n}$$

From (4), (15), and Table 1, the parameter A is estimated as $A \sim 0.034$.

6. TIME SCALES

Chu et al. [1990] found three time scales in the thermodynamically coupled oceanic and atmospheric boundary layers.

TABLE 1. Values of the Model Parameters

Parameter	Value
ρ_a	1.29 kg m^{-3}
h_c	5 cm
U_g	3 m s^{-1}
ρ_w	1035 kg m^{-3}
$\bar{T}_s$	28 °C
$\bar{S}$	35 g kg^{-1}
$\bar{h}_w$	50 m
α	0.2×10^{-3} K^{-1}
β	0.8×10^{-3}
C_1	1.0
C_2	0.2

6.1. *Fractional Cloudiness-Damping Time Scale*

$$\tau_n^{-1} = \frac{1}{h_c} \frac{\partial \bar{P}_r}{\partial n} \tag{29}$$

Using (4) and taking $h_c = 5$ cm, we have $\tau_n \sim 0.6$ day. Since n is interpreted as fractional cloudiness averaged over subgrid areas, the spatial scale for the fractional cloudiness-damping time scale is around 168 km.

6.2. *Ocean Mixed Layer Cooling Time Scale*

$$\tau_T^{-1} \equiv \frac{1}{\rho_w c_{pw} \bar{h}_w} \frac{\partial \bar{F}}{\partial T_s} \tag{30a}$$

On the basis of the assumption that θ_a and q in (12b) and (12c) are determined by the large-scale atmospheric motion only, from the surface heat balance equation (17a) we have

$$\tau_T^{-1} = \rho_a c_{pa} U_g \left(1 + \frac{L_v^2 q_s}{c_{pa} R_v \bar{T}_s^2} \frac{C_E}{C_H} + \frac{4 \sigma_{SB} \bar{T}_s^3}{\rho_a c_{pa} U_g C_H} \right) C_H \tag{30b}$$

6.3. *Cloud-SST Coupling Time Scale*

$$\tau_{n,T}^{-1} \equiv \frac{1}{\rho_w c_{pw} \bar{h}_w} \frac{\partial \bar{F}}{\partial n} \frac{\partial \bar{E}}{\partial \bar{T}_s^2} / [\xi (1 - \hat{e})]$$

This time scale $\tau_{n,T}$, is the time needed for the process that the deviation of fractional cloudiness, n', due to the change of ocean surface evaporation caused by SST variation, feeds back to SST through its effects on the surface heat flux. Utilization of (15), (16), and (27) leads to

$$\tau_{n,T}^{-1} = \left\{ \frac{\tau_n U_g L q_s [\partial (R_b - R_s) / \partial n]}{\rho_w c_{pw} h_w h_c R_v T_s^2} \right\} C_E \tag{31}$$

Among these three time scales, τ_n is the shortest. The other two, τ_T and $\tau_{n,T}$, depend on the parameters C_q, C_H, and C_E, which are functions of the atmospheric stability. Figure 3 shows the dependence of τ_T and $\tau_{n,T}$ on the atmospheric stability. For the unstable atmosphere ($h_a/L_a < 0$), $\tau_{n,T} \sim$ 3–6 days, and $\tau_T \sim$ 20–30 days. For the stable atmosphere ($h_a/L_a > 0$), $\tau_{n,T} \sim$ 0.3–1 years, and $\tau_T \sim$ 1–3 years.

The mean seasonal outgoing longwave radiation (OLR) consists of contributions from higher-frequency components of convection. *Lau and Chan* [1988] found two bands (1–5, 40–50 day) of oscillations in OLR. Large variability in the 1-

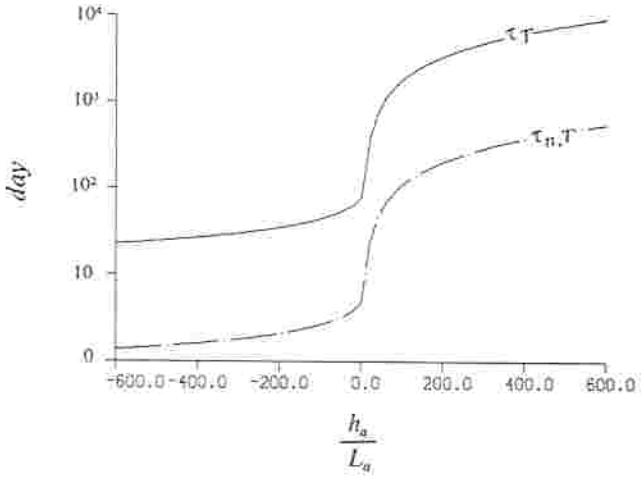

Fig. 3. Dependence of τ_T and $\tau_{n,T}$ on the atmospheric stability parameter (h_a/L_a).

to 5-day band is confined with the cloudy region distribution (e.g., equatorial western Pacific). The coincidence of these two bands with $\tau_{n,T}$ and τ_T for the unstable atmosphere (intense convection) indicates that τ_T (20- to 30-day time scale) is one of the intraseasonal variations.

The spectrum of average SST anomalies near the upper Peru Coast (4°–12°S) exhibits a major peak at 36.6–42.7 months, and a second peak at 10 months [*Rasmusson and Carpenter*, 1982]. The MABL near the Peru Coast is usually stable. The concurrence of these two peeks with $\tau_{n,T}$ (100–300 days) and τ_T (1–3 years) for the stable atmosphere may imply that our theoretical model is applicable to the low-frequency modes.

7. Model Parameters

Three nondimensional parameters are found important in the coupled system.

7.1. *Surface Stability Index*

The ocean mixed layer exhibits different behavior (entraining or shallowing), depending on the sign of the parameter:

$$\varepsilon = \frac{\tau_{n,T}(\bar{B}\bar{h}_w - C_1\bar{u}_{w*}^3/C_2)}{\beta g\bar{h}_w^2\bar{S}} \tag{32a}$$

When $\varepsilon > 0$, the ocean mixed layer is in the surface damping regime. When $\varepsilon < 0$, the ocean mixed layer is in the entrainment regime. In this study, we deal with the very low surface wind condition, which leads to

$$|\bar{B}| \gg \frac{C_1\bar{u}_{w*}^3}{C_2\bar{h}_w}$$

Therefore the surface damping factor is approximated by

$$\varepsilon \sim \frac{\tau_{n,T}\bar{B}}{\beta g\bar{h}_w\bar{S}} \tag{32b}$$

which means that the surface buoyancy flux is dominant over the surface wind forcing.

7.2. *Surface Water Budget Index*

The relative importance of surface freshwater influx in the surface buoyancy flux can be measured by the following parameter:

$$\gamma \equiv \frac{\beta g\bar{S}(\bar{P}_r - \bar{E})}{\bar{B}} \tag{33}$$

7.3. *Mean Diapycnal Gradient of Spiciness at Mixed Layer Base*

This parameter appears only in the entrainment regime. The definition of this parameter (δ) is given by (25). It is a tracer conserved by isentropic motions and an indicator of diffusive stability. It should be useful for the combined description of heat and salinity transfer in the entrainment zone.

8. Nondimensional Perturbation Equations

By using (28) and the definitions for the time scales ($\tau_{n,T}$, τ_T), (30*a*), (31), and for the model parameters γ, the perturbations of surface buoyancy and spiciness fluxes are

$$B' = -\frac{g\bar{h}_w}{2\rho_{w0}}[\tau_T^{-1} + \tau_{n,T}^{-1}(1 - A)](\chi' - \rho_w') + \frac{\bar{B}\gamma}{2\rho_{w0}\beta\bar{S}}(\chi' + \rho_w') \tag{34a}$$

$$D' = -\frac{g\bar{h}_w}{2\rho_{w0}}[\tau_T^{-1} + \tau_{n,T}^{-1}(1 - A)](\chi' - \rho_w') - \frac{\bar{B}\gamma}{2\rho_{w0}\beta\bar{S}}(\chi' + \rho_w') \tag{34b}$$

From (33) the ratio of the mean surface spiciness flux to mean surface buoyancy flux is

$$\frac{\bar{D}}{\bar{B}} = 1 - 2\gamma \tag{35}$$

Time t and the perturbations are nondimensionalized by

$$(t, \rho_w', \chi_w', h_w') = \left(\tau_T\bar{t}, \rho_{w0}\bar{\rho}_w, \rho_{w0}\bar{\chi}, \frac{g\bar{h}_w^2}{\bar{B}\tau_{n,T}}\bar{h}_w\right) \tag{36}$$

Assuming the upwelling velocity to be negligible, the nondimensional form of the perturbation equations (26*a*), (26*b*), and (26*c*) are

$$\frac{\partial\bar{\rho}_w}{\partial\bar{t}} = -\frac{1 + C_2\Lambda_w}{2}(1 + ma_+)\bar{\rho}_w + \frac{1 + C_2\Lambda_w}{2}(1 + ma_-)\bar{\chi} + (1 + C_2\Lambda_w)m\bar{h}_w \tag{37a}$$

$$\frac{\partial\bar{\chi}}{\partial\bar{t}} = \frac{1}{2}[1 + ma_- - C_2\Lambda_w\delta(1 + ma_+)]\bar{\rho}_w - \tfrac{1}{2}[1 + ma_+ - C_2\Lambda_w\delta(1 + ma_-)]\bar{\chi} - (1 - 2\gamma - C_2\Lambda_w\delta)m\bar{h}_w \tag{37b}$$

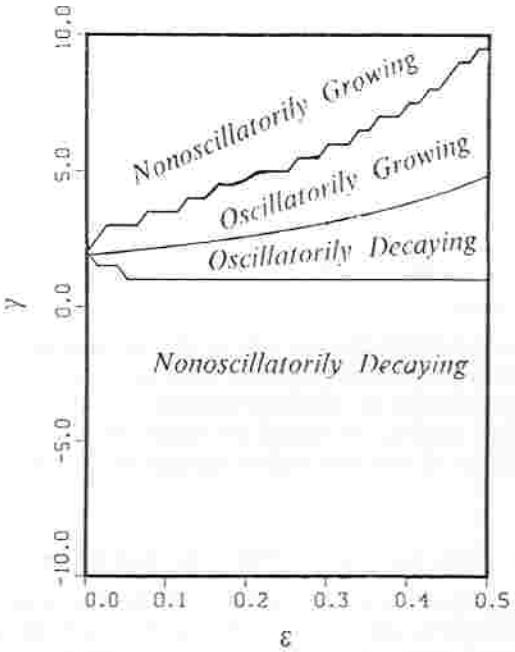

Fig. 4. Separation of modes in the (ε, γ) plane for the surface damping regime $(\varepsilon > 0)$.

$$\Lambda_w \frac{\mu}{\varepsilon} \frac{\partial \bar{h}_w}{\partial \bar{t}} = C_2 m \bar{h}_w + \frac{C_2}{2}(1 + m a_+)\bar{\rho}_w - \frac{C_2}{2}(1 + m a_-)\bar{\chi} \qquad (37c)$$

where

$$a_+ \equiv 1 - A + \varepsilon\gamma \qquad a_- \equiv 1 - A - \varepsilon\gamma$$

$$m \equiv \frac{\tau_T}{\tau_{n,T}} \qquad \mu \equiv \frac{\Delta\rho_w}{\rho_{w0}\beta S} \qquad (38)$$

Only three parameters in the basic system (37*a*), (37*b*), and (37*c*) are allowed to vary: ε, γ, and δ. The others are fixed: $A \sim 0.034$, $m \sim 3$–5, and $\mu \sim -0.01$.

9. Solutions

The system (37*a*), (37*b*), and (37*c*) contains both surface damping ($\Lambda_w = 0$) and entrainment ($\Lambda_w = 1$) regimes. The general solutions of the basic system (37*a*), (37*b*), and (37*c*) have the form

$$(\bar{\rho}_w, \bar{\chi}, \bar{h}_w) \sim \Sigma(D_{\rho j}, D_{\chi j}, D_{hj})e^{\sigma_j t} \qquad (39)$$

where $D_{\rho j}, D_{\chi j}, D_{hj} (j = 1, 2, \cdots)$ are the integral constants, and σ_j are eigenvalues, which are roots of an algebraic equation. It is noteworthy that for the entrainment regime ($\Lambda_w = 1$), this algebraic equation is of the third order, whereas for the damping regime ($\Lambda_w = 0$), it is of the second order. This order change is attributable to the change from prognostic to diagnostic form for the respective mixed layer depth equations (37*c*). Therefore in the solution (39), there are two terms for the surface damping regime and three terms for the entrainment regime.

10. Instability and Oscillation Criteria

The instability criterion for the thermodynamically coupled air-ocean system is

$$\begin{aligned} \sigma_r &\equiv \mathrm{Re}\,(\sigma) < 0 && \text{decaying} \\ \sigma_r &\equiv \mathrm{Re}\,(\sigma) = 0 && \text{neutral} \\ \sigma_r &\equiv \mathrm{Re}\,(\sigma) > 0 && \text{growing} \end{aligned} \qquad (40)$$

The oscillation criterion for the coupled system is

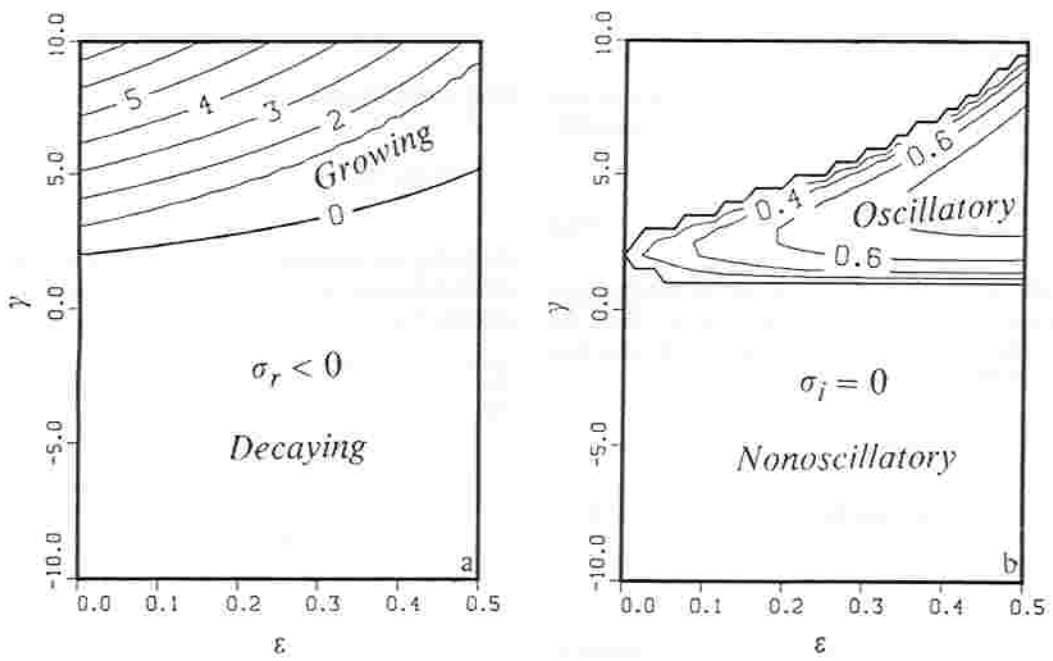

Fig. 5. Eigenvalue σ in the (ε, γ) plane for the surface damping regime $(\varepsilon > 0)$: (*a*) σ_r; (*b*) $|\sigma_i|$.

$$\sigma_i \equiv \mathrm{Im}\,(\sigma) = 0 \qquad \text{nonoscillatory}$$
$$\sigma_i \equiv \mathrm{Im}\,(\sigma) \neq 0 \qquad \text{oscillatory} \tag{41}$$

We should keep in mind that the linear theory is valid only for infinitesimally small perturbations, i.e., $|(\ )'| \ll |\overline{(\ )}|$. As the perturbations become sufficiently large, this requirement is no longer satisfied; therefore the solutions are no longer valid. We must then consider the nonlinear system.

10.1. *Shallowing Regime ($\varepsilon > 0$)*

In this regime ($\Lambda_w = 0$), substitution of (39) into (37*a*), (37*b*), and (37*c*) leads to a quadratic equation of σ:

$$[\sigma + (1 + ma_+)]\left\{\sigma + \frac{1}{2}[1 + ma_+ + (1 + ma_-)(1 - 2\gamma)]\right\} + \frac{1}{2}[1 + ma_- + (1 + ma_+)(1 - 2\gamma)](1 + ma_-) = 0 \tag{42}$$

It is notable in (42) that the parameter δ does not appear in the surface damping regime. There are two roots of σ at each pair of given values of model parameters (ε, γ). Between the two roots, the first one always has a negative real part through the whole ε-γ plane, representing damping modes, which are not of interest and are neglected. The second root has a positive real part in some domains of the ε-γ plane. The properties of this root indicate different modes according to its real (σ_r) and imaginary (σ_i) parts

$$\begin{aligned} &\sigma_r > 0 \qquad \sigma_i = 0 \Rightarrow \text{nonoscillatorily growing} \\ &\sigma_r > 0 \qquad \sigma_i \neq 0 \Rightarrow \text{oscillatorily growing} \\ &\sigma_r < 0 \qquad \sigma_i \neq 0 \Rightarrow \text{oscillatorily decaying} \\ &\sigma_r < 0 \qquad \sigma_i = 0 \Rightarrow \text{nonoscillatorily decaying} \end{aligned} \tag{43}$$

Figure 4 shows the separation of different modes in the (ε-γ) plane. The three lines (if small fluctuations are ignored) divide the (ε, γ) plane into four modes:

$$\begin{aligned} &\gamma > f_1(\varepsilon) \Rightarrow \text{nonoscillatorily growing} \\ &f_1(\varepsilon) > \gamma > f_2(\varepsilon) \Rightarrow \text{oscillatorily growing} \\ &f_2(\varepsilon) > \gamma > f_3(\varepsilon) \Rightarrow \text{oscillatorily decaying} \\ &\gamma < f_3(\varepsilon) \Rightarrow \text{nonoscillatorily decaying} \end{aligned} \tag{44}$$

where

$$\begin{aligned} &f_1(\varepsilon) \approx 2 + 15\varepsilon \qquad f_2(\varepsilon) \approx 2 + 6\varepsilon \\ &f_3(\varepsilon) \approx 2 - 20\varepsilon\,(\varepsilon < 0.05) \qquad f_3(\varepsilon) \approx 1\,(\varepsilon > 0.05) \end{aligned} \tag{45}$$

The model parameter, γ, represents the relative importance of the net surface freshwater influx in the mean buoyancy flux $\bar{B}$ and indicates the strength of positive feedback mechanism between the coupled system. On the other hand, the surface damping factor (ε) denotes the negative feedback mechanism. When $\gamma > f_1(\varepsilon)$, the positive feedback mechanism dominates the negative feedback mechanism, and the prognostic variables ($\bar{\rho}_w$, $\bar{\chi}$) increase exponentially with the growth rate $\sigma_r \sim 3$–5 (in units of τ_T^{-1}). The time during which the perturbations of density (ρ_w') and of the spiciness (χ) double their strengths is

$$T_{\text{double}} = \frac{\ln 2}{\sigma_r} \sim 0.2\tau_T$$

When $f_1(\varepsilon) > \gamma > f_3(\varepsilon)$, the positive and negative feedback mechanisms are comparable. Because of phase differences, the corresponding modes are oscillatory. If γ is sufficiently large, i.e., $\gamma > f_2(\varepsilon)$, the positive feedback mechanism caused by the net surface freshwater influx prevails, and the system is oscillatory and unstable. The growth ranges from $0 - 1\tau_T^{-1}$ (Figure 5*a*), and the period of the oscillation is the order of $2\pi\tau_T$ (Figure 5*b*). However, for $\gamma < f_2(\varepsilon)$, the negative feedback mechanism dominates, and the initial perturbations will be damped. Furthermore, (37*c*) shows that in the entrainment regime ($\Lambda_w = 1$), if the density jump at the mixed layer base, $\Delta\rho_w$, is infinitesimally small, the local time rate of change of the mixed layer depth will be negligible. Equation (37*c*) is the same as for the surface damping regime. Therefore when the mixed layer depth is predicted to increase by (37*c*) for the surface damping regime ($\Lambda_w = 0$), the regime switches to the entrainment regime, with negligible density and spiciness jumps assumed at the base of the mixed layer.

10.2. *Entrainment Regime ($\varepsilon < 0$)*

For the low wind speed case, the inequality, $\varepsilon < 0$, is approximately equivalent to $\bar{B} < 0$. The parameter γ is negative (positive) when the mean precipitation rate ($\bar{P}_r$) exceeds (lags) the mean surface evaporation rate ($\bar{E}$). The basic system (37*a*), (37*b*), and (37*c*) of this regime is a set of three first-order ordinary equations. Substitution of (39) into (37*a*), (37*b*), and (37*c*) leads to ($\Lambda_w = 1$) a third-order algebraic equation for the eigenvalue σ:

$$\begin{vmatrix} A_{11} - \sigma & A_{12} & A_{13} \\ A_{12} & A_{22} - \sigma & A_{23} \\ A_{31} & A_{32} & A_{33} - \sigma \end{vmatrix} = 0 \tag{46}$$

where

$$\begin{aligned} A_{11} &= -\frac{1 + C_2}{2}(1 + ma_+) \\ A_{12} &= \frac{1 + C_2}{2}(1 + ma_-) \\ A_{13} &= (1 + C_2)m \\ A_{21} &= \frac{1}{2}[1 + ma_- - C_2\delta(1 + ma_+)] \\ A_{22} &= -\frac{1}{2}[1 + ma_+ - C_2\delta(1 + ma_-)] \\ A_{23} &= -(1 - 2\gamma - C_2\delta)m \\ A_{31} &= \frac{C_2\varepsilon}{2\mu}(1 + ma_+) \\ A_{32} &= -\frac{C_2\varepsilon}{2\mu}(1 + ma_-) \\ A_{33} &= \frac{C_2\varepsilon m}{\mu} \end{aligned} \tag{47}$$

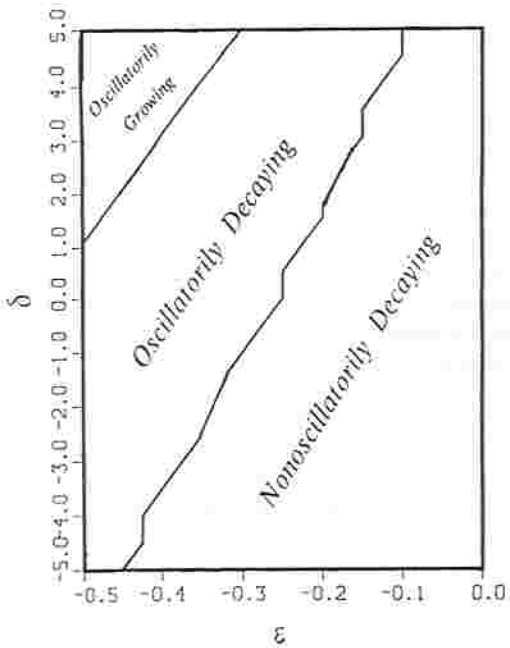

Fig. 6. Separation of modes in the (ε, δ) plane for the entrainment regime ($\varepsilon < 0$) for $\gamma = -0.1$.

There are three roots of σ for each set of model parameters (ε, γ, δ). Among the three roots, the first always has a negative real part and represents damping mode that is not of interest here. The other two roots, in certain domains, are complex conjugates, representing the same oscillatory modes. In other domains, they are both real, representing the nonoscillatory modes. The eigenvalue with a larger real part will be discussed in this section. The distributions of σ_r and σ_i control the properties of the modes, as shown in (43). The solutions show that only damping modes are available when the surface evaporation rate $\bar{E}$ exceeds the precipitation rate $\bar{P}_r$. In the low mean wind speed region, the entrainment process is mainly driven by upward buoyancy flux (i.e., $\bar{B} < 0$). From the definition of γ (33), the bigger absolute value of γ implies the weaker entrainment process. For a not very weak entrainment process (i.e., $|\gamma|$ is not too large), the solution greatly depends on the mean diapycnal gradient of spiciness in the entrainment zone, δ. We compute the eigenvalues in the (ε, δ) plane for several negative values of γ: -0.1, -0.2, and -0.5, as shown in Figures 6–8. In the entrainment regime ($\varepsilon < 0$), the net freshwater influx makes $\gamma < 0$. In such a case ($\varepsilon < 0$, $\gamma < 0$), the parameter δ will play a key role in determining the stability of the coupled system. When δ exceeds a criterion that varies with ε and γ, the oscillatory growing modes will be generated. The model results show the criteria to be $\delta > 20\varepsilon + 11$ for $\gamma = -0.1$ (Figure 6), $\delta > 20\varepsilon + 11.8$ for $\gamma = -0.2$ (Figure 7), and $\delta > 20\varepsilon + 14.6$ for $\gamma = -0.5$ (Figure 8). The shrinkage of the unstable oscillation area with the decrease in γ (from -0.1 to -0.5) implies that (1) the more the net freshwater influx, or (2) the weaker the entrainment process, the stronger the salinity stratification domination should be in the entrainment zone.

The distributions of the real and imaginary parts of the eigenvalue σ_r, $|\sigma_i|$ for different values of γ are shown in Figure 9 ($\gamma = -0.1$), Figure 10 ($\gamma = -0.2$), and Figure 11 ($\gamma = -0.5$). If our interests are only in the unstable modes, representing the enhancement of initial perturbations, these figures indicate the following:

1. In the unstable region, the decrease of parameter γ (from -0.1 to -0.5) decreases the growth rate σ_r and increases the frequency $|\sigma_i|$ (1.5 to 3.5 τ_T^{-1}). This indicates that the ability of the net freshwater influx (represented by the negative value of γ) to amplify the initial perturbation is reduced when the entrainment process weakens.

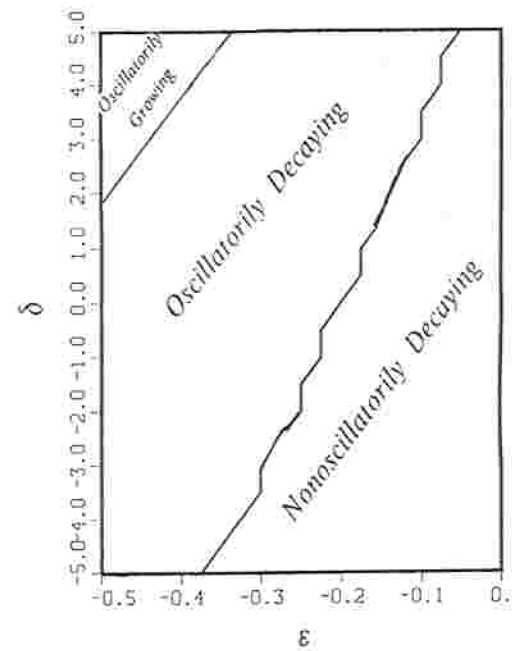

Fig. 7. Separation of modes in the (ε, δ) plane for the entrainment regime ($\varepsilon < 0$) for $\gamma = -0.2$.

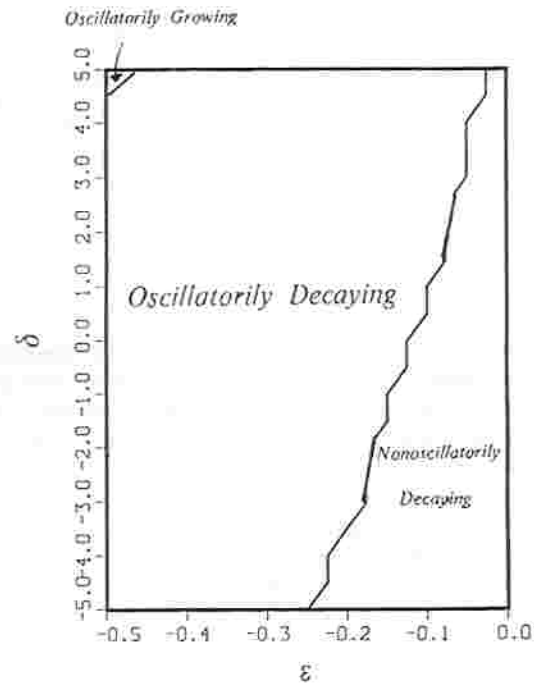

Fig. 8. Separation of modes in the (ε, δ) plane for the entrainment regime ($\varepsilon < 0$) for $\gamma = -0.5$.

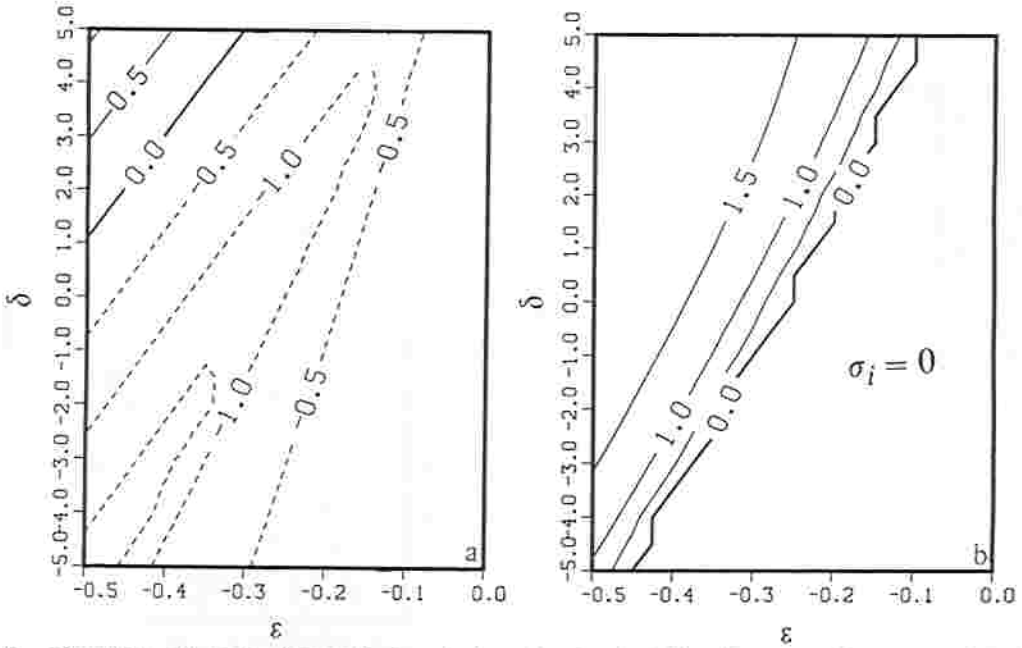

Fig. 9. Eigenvalue σ in the (ε, δ) plane for the entrainment regime $(\varepsilon < 0)$ and for $\gamma = -0.1$: (*a*) σ_r, and (*b*) $|\sigma_i|$.

2. The unstable oscillation only appears as $\delta > 0$, which means that the net surface freshwater influx generates the unstable modes only in the salinity stratification–dominated entrainment zone.

3. When the entrainment zone is dominated by temperature stratification, the net surface freshwater influx can only dampen the initial perturbation.

11. CONCLUSIONS

The feedback between the cloud and OPBL in the coupled MABL and hydrodynamically stable OPBL system is investigated by a simple one-dimensional coupled model. The time scales largely depend on the stability of the MABL. For the stable atmosphere, the two time scales are quite long: $\tau_{n,T} \sim$ 100–300 days, and $\tau_T \sim$ 1–3 yr. For the unstable atmosphere, however, the two time scales are much shorter: $\tau_{n,T} \sim$ 3–6 days, and $\tau_T \sim$ 20–30 days. In the western Pacific warm pool regions, the MABL is usually unstable. Therefore this theory may provide some explanation for the two time scales (3–6 and 20–30 days) of intense atmospheric convection above the western Pacific warm pool.

The mean freshwater influx at the ocean surface due to the excess precipitation over evaporation amplifies the initial perturbations.

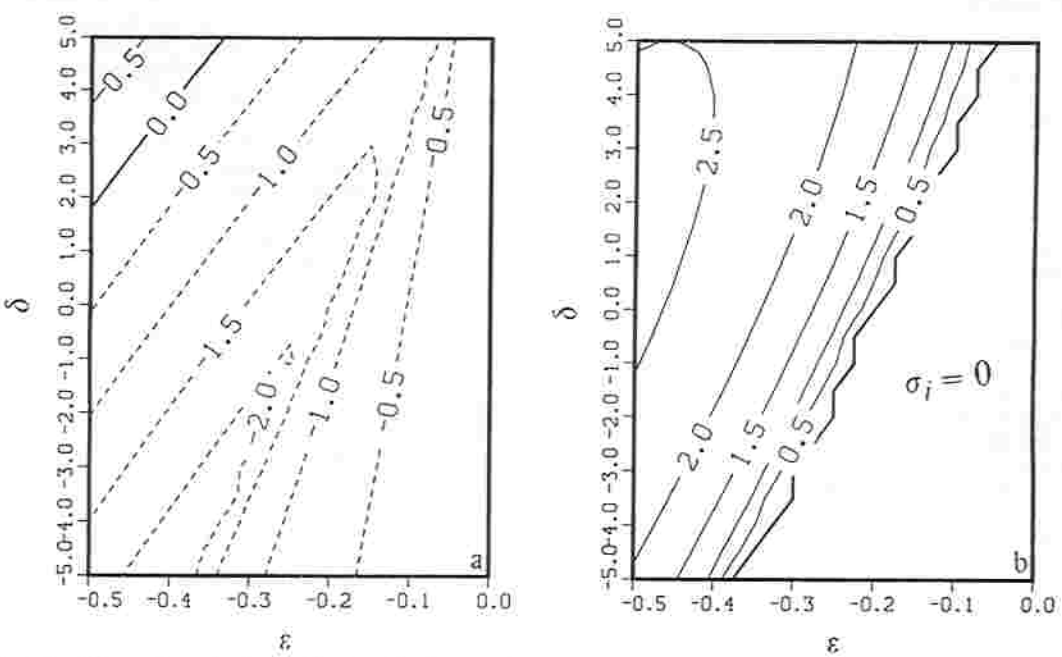

Fig. 10. Eigenvalue σ in the (ε, δ) plane for the entrainment regime $(\varepsilon < 0)$ and for $\gamma = -0.2$: (*a*) σ_r, and (*b*) $|\sigma_i|$.

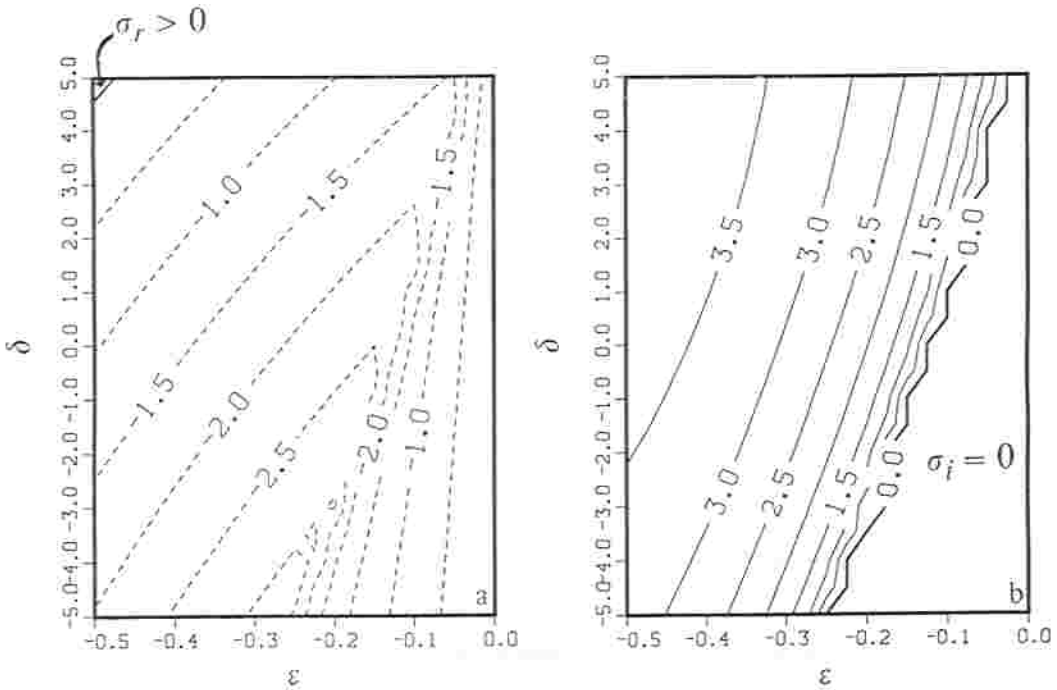

Fig. 11. Eigenvalue σ in the (ε, δ) plane for the entrainment regime $(\varepsilon < 0)$ and for $\gamma = -0.5$: (*a*) σ_r, and (*b*) $|\sigma_i|$.

In the entrainment regime, the mean diapycnal gradient in the entrainment zone δ plays an important role in determining the instability of the coupled system. When δ exceeds a criterion that varies with ε and γ, the oscillatorily growing modes will be generated. The model results show that the criteria are $\delta > 20\varepsilon + 11$ for $\gamma = -0.1$, $\delta > 20\varepsilon + 11.8$ for $\gamma = -0.2$, and $\delta > 20\varepsilon + 14.6$ for $\gamma = -0.5$.

Furthermore, the dynamics of the ocean mixed layer is highly nonlinear. There is no smooth transition between the entrainment and the surface damping regimes. The use of the linear theory enables our initial search for feedback mechanisms. The nonlinear effects should be take into account in realistic applications.

Acknowledgments. This research was supported by the National Science Foundation, the Office of Naval Research, and the Naval Postgraduate School. We appreciate the efforts of Arlene Bird in improving the manuscript.

REFERENCES

Albright, M. D., E. E. Recker, R. J. Reed, and R. Q. Dang, The diurnal variation of deep convection and inferred precipitation in the central tropical Pacific during January–February 1979, *Mon. Weather Rev.*, *113*, 1663–1680, 1985.

Arkin, P. A., The relationship between fractional coverage of high cloud and rainfall accumulations during GATE over the B-scale array, *Mon. Weather Rev.*, *107*, 1382–1387, 1979.

usinger, J. A., J. C. Wyngaard, Y. Izumi, and E. F. Bradley, Flux profile relationships in the atmospheric surface layer, *J. Atmos. Sci.*, *28*, 181–189, 1971.

nu, P. C., and R. W. Garwood, Jr., Comment on "A coupled dynamic-thermodynamic model of an ice-ocean system in the marginal ice zone" by S. Häkkinen, *J. Geophys. Res.*, *93*, 5155–5156, 1988.

Chu, P. C., and R. W. Garwood, Jr., Cloud-ocean mixed layer feedback, paper presented at AMS Symposium on the Role of Clouds in Atmospheric Chemistry and Global Climate, Am. Meteorol. Soc., Los Angeles, Calif., 1989.

Chu, P. C., and R. W. Garwood, Jr., Thermodynamical feedback between clouds and ocean mixed layer, *Adv. Atmos. Sci.*, *7*, 1–10, Springer-Verlag, New York, 1990.

Chu, P. C., R. W. Garwood, Jr., and P. Muller, Unstable and damped modes in coupled ocean mixed layer and cloud models, *J. Mar. Syst.*, *1*, 1–11, 1990.

Davey, M. K., Results from a moist equatorial atmosphere model, in *Coupled Ocean-Atmosphere Models, Elsevier Oceanogr. Ser.*, vol. 40, edited by J. Nihoul, pp. 41–49, 1985.

Gill, A. E., Some simple solutions for heat induced tropical circulation, *Q. J. R. Meteorol. Soc.*, *106*, 447–462, 1980.

Kuo, H. L., On formation and intensification of tropical cyclones through latent heat release by cumulus convection, *J. Atmos. Sci.*, *22*, 40–63, 1965.

Lau, K. M., and P. H. Chan, Intraseasonal and interannual variations of tropical convection: A possible link between 40–50 day oscillation and ENSO?, *J. Atmos. Sci.*, *45*, 506–521, 1988.

Lau, K. M., and S. Shen, On the dynamics of intraseasonal oscillation and ENSO, *J. Atmos. Sci.*, *45*, 1781–1797, 1988.

Munk, W., Internal waves and small-scale processes, *Evolution of Physical Oceanography*, pp. 264–291, MIT Press, Cambridge, Mass., 1981.

Rasmusson, E. M., and T. H. Carpenter, Variations in tropical sea surface temperature and surface wind fields associated with the Southern Oscillation/El Nino, *Mon. Weather Rev.*, *110*, 354–384, 1982.

Sadler, J. C., M. A. Lander, A. M. Hori, and L. K. Oda, Tropical marine climatic atlas, vol. II, Pacific Ocean, *Rep. UHMET87-02*, 27 p., Univ. of Hawaii, Honolulu, 1987.

Stephens, G. L., Aspects of cloud-climate feedback, paper presented at AMS Symposium on the Role of Clouds in Atmospheric Chemistry and Global Climate, Am. Meteorol. Soc., Los Angeles, Calif., 1989.

Veronis, G., On properties of seawater defined by temperature, salinity, and pressure, *J. Mar. Res.*, *30*, 227–255, 1972.

Yamada, T., On the similarity functions A, B, and C of the planetary boundary layer, *J. Atmos. Sci.*, *33*, 781–793, 1976.

Wyrtki, K., and G. Meyers, The trade wind field over the Pacific Ocean, *J. Appl. Meteorol.*, *15*, 698–704, 1976.

P. C. Chu and R. W. Garwood, Jr., Department of Oceanography, Naval Postgraduate School, Monterey, CA 93943.

(Received January 22, 1990.
accepted July 23, 1990.)